multiple formation of tumor in the small intestines of *Mutyh*-deficient mice provides a suitable model system to investigate the processes of intestinal tumorigenesis.

Xie *et al.* showed that *Mutyh/Ogg1* double-deficient mice predominantly developed lung and ovarian tumors as well as lymphomas. They also showed that 8.6% of *Mutyh/Ogg1* double-deficient mice exhibited adenomas/carcinomas in their gastrointestinal tracts, which were not observed in wild-type mice[7]. We and other groups have previously reported that there was little difference in the number of intestinal tumors in wild-type and Ogg1-null mice, although an Ogg1 deficiency resulted in 8-oxoG buildup in genomic DNA and an elevated mutation frequency in the latter[4,8,9]. Thus, the development of intestinal tumors in *Mutyh/Ogg1* double-deficient mice supports the notion that having a Mutyh deficiency does indeed increase susceptibility to intestinal tumorigenesis regardless of the genetic background or environmental factors.

I. $KBrO_3$-induced intestinal tumors in wild-type and *Mutyh*-deficient mice

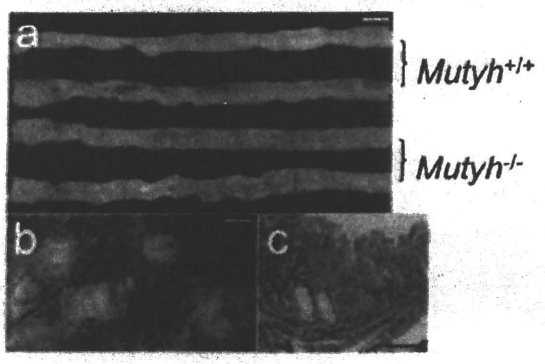

II.Frequency of $KBrO_3$-induced intestinal tumors in wild-type and *Mutyh*-deficient mice (tumors/mouse)

Genotype	Sex	Mean ± S.D.
Mutyh +/+	♂	0.50 ± 0.55
	♀	1.00 ± 0.71
Mutyh -/-	♂	72.75 ± 24.24
	♀	51.00 ± 28.35

Figure 2 $KBrO_3$-induced tumors in the small intestine of *Mutyh*-deficient mice.
I. a, The upper part of the small intestines (duodenum and a part of jejunum) from $KBrO_3$-treated mice are shown. Multiple polyp formations are observed in the $KBrO_3$-treated *Mutyh*-deficient mice (-/-), but not in the treated wild-type mice (+/+). Upper: female, lower: male. b, A high-power view of the polyps in the $KBrO_3$-treated *Mutyh*-deficient female mouse. c, A section of the $KBrO_3$-induced polyp stained with haematoxylin and eosin. Scale bars; a: 1 cm, b: 1 mm, c: 100 μm. II. $KBrO_3$ was administered to wild-type and *Mutyh*-deficient mice in their drinking water for 16 weeks. Body weight and water consumption were monitored weekly. The animals were sacrificed at the age of 20 weeks, and their intestines were removed and fixed in 4% paraformaldehyde fixative. Microscopic inspection for tumor formation was performed (adopted from reference 5).

1) Familial adenomatous polyposis with a recessive trait

- Patients have germ-line mutations in the *MUTYH* gene (About 80% of the mutations were identified as Y165C or G382D in the patients of Europe and USA)
- Onset: 50 years of age (median, range:16~59 years of age) *
- No. of tumors: 40/colon(median, range: 18~100 tumors) *
- *United Kingdom patients (156) with multiple (5~100) adenomas

2) Tumors from the patients all showed G:C to T:A mutations in the *APC* gene.

3) Almost all the G:C to T:A mutations occur in the GAA sequence context of the *APC* gene

Figure 3 MutYH-associated polyposis (MAP).

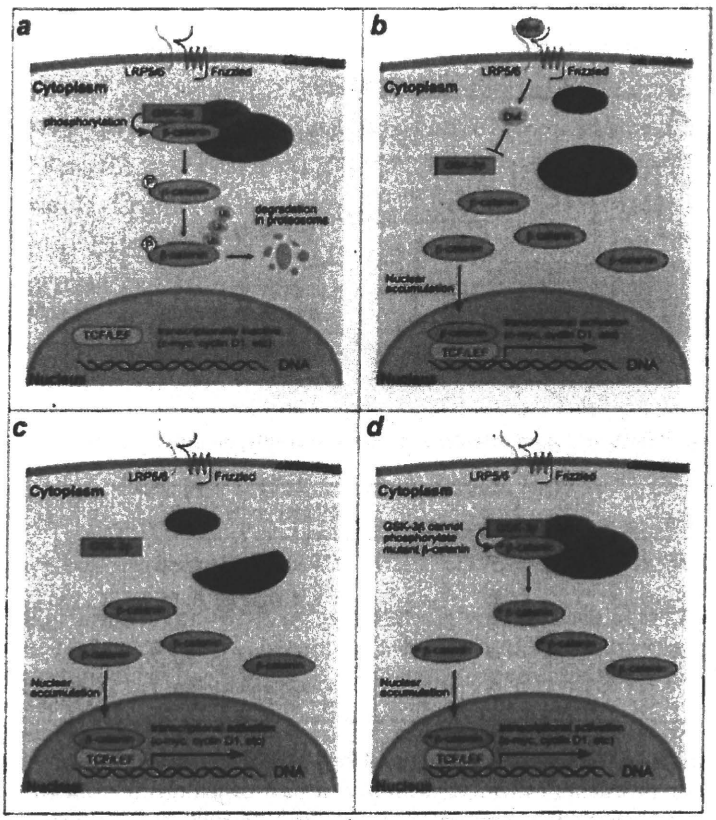

Figure 4 Wnt signaling pathway (canonical).
a) In the absence of Wnt signaling, β-catenin is phosphorylated by GSK3β in a complex with axin and Apc, and is subsequently ubiqutinated and degradated in the proteasome. *b*) In the presence of Wnt signaling, activated Dishevelled (Dvl) inhibits phoshorylation of β-catenin, consquently leading to stabilization of β-catenin. Nuclear accumulated β-catenin activates transcription of the target genes. Mutations in either APC (*c*) or in the phosphorylation sites of β-catenin (*d*) abolish the phoshorylation of β-catenin, which in turn leads to an accumulation of nuclear β-catenin, thereby up-regulating the expression of the target genes without Wnt signaling, and resulting in carcinogenic cell growth.

It is of interest that the deficiency of Mutyh but not Ogg1 makes mice susceptible to intestinal tumorigenesis, although the deficiency of either Mutyh or Ogg1 increases G:C to T:A transversion at almost equal frequency in the small intestines of mice. It is possible that this difference may be attributed to the additional substrate; MUTYH excises 2-hydroxyadenine, an oxidized adenine, paired with guanine, beside adenine paired with 8-oxoguanine, from DNA. However, we recently reported the involvement of Mutyh in cell death caused by oxidative DNA damage[10]. Thus, the defect in Mutyh would simultaneously compromise both DNA repair and cell-death induced by oxidative DNA damage (Figure 5). This may explain why among the factors involved in suppressing oxidative damage-induced mutagenesis, only MUTYH is, so far, identified to be associated with hereditary colorectal cancers in humans.

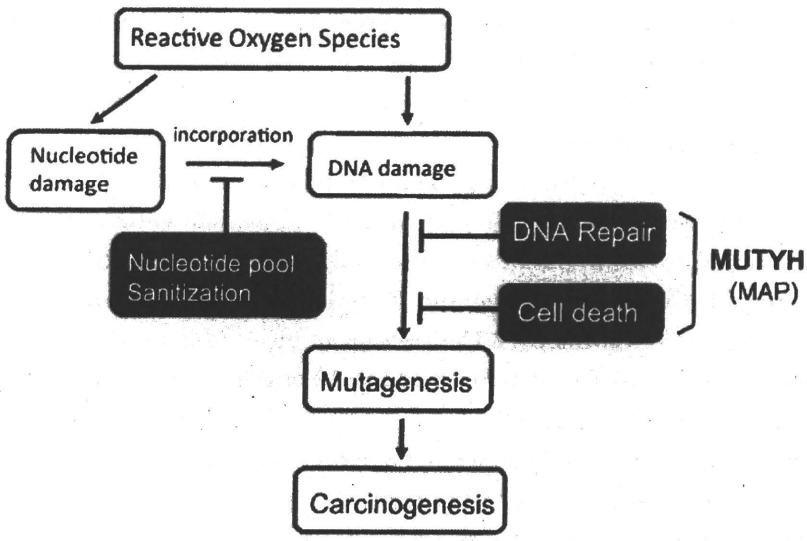

Figure 5 The roles of MUTYH in the avoiding mechanisms for ROS-induced mutagenesis and carcinogenesis.
The defect in Mutyh simultaneously compromise both DNA repair and cell-death induced by oxidative DNA damage. Thus, the defect in Mutyh makes mice highly susceptible to oxidative stress-induced tumorigenesis. This may provide molecular bases for explaining why among the factors involved in suppressing oxidative damage-induced mutagenesis, only MUTYH is, so far, identified to be associated with hereditary colorectal cancers in humans.

References

1. Sekiguchi M, Tsuzuki T. Oxidative nucleotide damage: consequences and prevention. Oncogene, 21: pp.8895-8904, 2002
2. Tsuzuki T, Nakatsu Y, Nakabeppu Y. Significance of error-avoiding mechanisms for oxidative DNA damage in carcinogenesis. Cancer Sci, 98: pp.465-470, 2007
3. Tsuzuki T, Egashira A, Igarashi H, Iwakuma T, Nakatsuru Y, Tominaga Y, Kawate H, Nakao K, Nakamura K, Ide F, Kura S, Nakabeppu Y, Katsuki M, Ishikawa T, Sekiguchi M. Spontaneous tumorigenesis in mice defective in the *MTH1* gene encoding 8-oxo-dGTPase. Proc. Natl. Acad. Sci. USA, 98: pp.11456-11461, 2001
4. Sakumi K, Tominaga Y, Furuichi M, Xu P, Tsuzuki T, Sekiguchi M, Nakabeppu Y, *Ogg1* knockout-associated lung tumorigenesis and its suppression by *Mth1* gene disruption. Cancer Res, 63: pp.902-905, 2003
5. Sakamoto K, Tominaga Y, Yamauchi K, Nakatsu Y, Sakumi K, Yoshiyama K, Egashira A, Kura S, Yao T, Tsuneyoshi M, Maki H, Nakabeppu Y, Tsuzuki, T. MUTYH-null mice are susceptible to spontaneous and oxidative stress-induced intestinal tumorigenesis. Cancer Res., 67: pp.6599-6604, 2007
6. Al-Tassan N, Chmiel N H, Maynard J, Fleming N, Livingston AL, Williams GT, Hodges AK, Davies DR, David SS, Sampson JR, Cheadle JP. Inherited variants of MYH associated with somatic G:C to T:A mutations in colorectal tumors. Nat Genet, 30: pp.227-232, 2002
7. Xie Y, Yang H, Cunanan C, Okamoto K, Shibata D, Pan J, Barnes DE, Lindahl T, McIlhatton M, Fishel R, Miller JH. Deficiencies in mouse *Myh* and *Ogg1* result in tumor predisposition and G to T mutations in codon 12 of the K-ras oncogene in lung tumors. Cancer Res, 64: pp.3096–3092, 2004
8. Klungland A, Rosewell I, Hollenbach S, Larsen E, Daly G, Epe B, Seeberg E, Lindahl T, Barnes DE. Accumulation of premutagenic DNA lesions in mice defective in removal of oxidative base damage. Proc. Natl. Acad. Sci .USA, 96: pp.13300–13305. 1999
9. Minowa O, Arai T, Hirano M, Monden Y, Nakai S, Fukuda M, Itoh M, Takano H, Hippou Y, Aburatani H, Masumura K, Nohmi T, Nishimura S, Noda T. *Mmh/Ogg1* gene inactivation results in accumulation of 8-hydroxyguanine in mice. Proc. Natl Acad. Sci. USA, 97: pp.4156–4161, 2000
10. Oka S, Ohno M, Tsuchimoto D, Sakumi K, Furuichi M, Nakabeppu Y. Two distinct pathways of cell death triggered by oxidative damage to nuclear and mitochondrial DNAs. EMBO J, 27: pp.421-432 2008

Acknowledgments

This work was supported by grants from the Ministry of Education, Culture, Sports, Scinece and Technology, the Ministry of Health, Labor and Welfare of Japan, and the Japan Society for the Promotion of Science.

Dr. Teruhisa Tsuzuki, D.Sc.

1982-1990	Research Associate, Department of Biochemistry, Kumamoto University Medical School
1988-1992	Research Associate, Howard Hughes Medical Institute, The University of Utah, U.S.A.
1992-1998	Associate Professor, Department of Biochemistry, Medical Institute of Bioregulation, Kyushu University
1998-	Professor, Department of Medical Biophysics and Radiation Biology, Faculty of Medical Sciences, Kyushu University

Specialty and Present Interest:
Oxidative DNA damage, Mutagenesis and Tumorigenesis, Gastrointestinal Tumor

Genes, Brain and Behavior
Official publication of the International Behavioural and Neural Genetics Society

Genes, Brain and Behavior (2010)

Comprehensive behavioural study of GluR4 knockout mice: implication in cognitive function

N. Sagata[†], A. Iwaki[†], T. Aramaki[†], K. Takao[‡,§,¶], S. Kura[**], T. Tsuzuki[**], R. Kawakami[††], I. Ito[††], T. Kitamura[††], H. Sugiyama[††], T. Miyakawa[‡,§,¶] and Y. Fukumaki[*,†]

[†]Division of Human Molecular Genetics, Research Center for Genetic Information, Medical Institute of Bioregulation, Kyushu University, Fukuoka, [‡]Laboratory for Genetic Engineering and Functional Genomics, Frontier Technology Center, Kyoto University Faculty of Medicine, Kyoto, [§]Japan Science and Technology Agency (JST), Institute for Bioinformatics Research and Development (BIRD), Core Research for Evolutional Science and Technology (CREST), Kawaguchi, [¶]Division of Systems Medical Science, Institute for Comprehensive Medical Science, Fujita Health University, Toyoake, and [**]Department of Medical Biophysics & Radiation Biology and [††]Department of Biology, Faculty of Science, Kyushu University, Fukuoka, Japan
**Corresponding author: Y. Fukumaki, Division of Human Molecular Genetics, Research Center for Genetic Information, Medical Institute of Bioregulation, Kyushu University, 3-1-1 Maidashi, Higashi-ku, Fukuoka 812-8582, Japan. E-mail: yfukumak@gen.kyushu-u.ac.jp*

Fast excitatory transmission in the mammalian central nervous system is mediated by AMPA-type glutamate receptors. The tetrameric AMPA receptor complexes are composed of four subunits, GluR1–4. The GluR4 subunit is highly expressed in the cerebellum and the early postnatal hippocampus and is thought to be involved in synaptic plasticity and the development of functional neural circuitry through the recruitment of other AMPA receptor subunits. Previously, we reported an association of the human GluR4 gene (*GRIA4*) with schizophrenia. To examine the role of the GluR4 subunit in the higher brain function, we generated GluR4 knockout mice and conducted electrophysiological and behavioural analyses. The mutant mice showed normal long-term potentiation (LTP) in the CA1 region of the hippocampus. The GluR4 knockout mice showed mildly improved spatial working memory in the T-maze test. Although the retention of spatial reference memory was intact in the mutant mice, the acquisition of spatial reference memory was impaired in the Barnes circular maze test. The GluR4 knockout mice showed impaired prepulse inhibition. These results suggest the involvement of the GluR4 subunit in cognitive function.

Keywords: AMPA receptors, cognitive function, GluR4, knockout mice, prepulse inhibition, schizophrenia

Received 23 March 2010, revised 8 June 2010 and 14 July 2010, accepted for publication 14 July 2010

GluR4 is a subunit of α-amino-3-hydroxy-5-methyl-4-isoxazolepropionic acid (AMPA) receptors that mediate fast synaptic excitatory neurotransmission in the mammalian central nervous system (CNS). The AMPA receptors are ligand-gated ionotropic receptors and are important for the expression of several forms of long-lasting synaptic plasticity including long-term potentiation (LTP) and long-term depression (LTD) (Bear & Abraham 1996; Bliss & Collingridge 1993; Malenka & Nicoll 1999). GluR4 and other AMPA receptor subunits, GluR1–3 (also referred to as GluRD and GluRA–C), assemble into a tetrameric complex to form a functional channel (Mano & Teichberg 1998; Mansour *et al.* 2001; Rosenmund *et al.* 1998). GluR4 subunit expression is distributed throughout the CNS, but is relatively high in the CA1 and the dentate gyrus of the hippocampus, layers III and IV of the cerebral cortex and the granule cells of the cerebellum (Keinänen *et al.* 1990). Especially in the hippocampus, high GluR4 expression is largely restricted to the first postnatal week, and the GluR4 subunit mediates the delivery of GluR2-containing AMPA receptors (Zhu *et al.* 2000). Thus, the GluR4 subunit may be responsible for the function of the early postnatal hippocampus through the initial establishment of long-lasting functional circuitry. Early neonatal inactivation of the hippocampus with ibotenic acid alters the development and plasticity of the prefrontal cortical circuitry and produces behavioural and cellular changes that mimic many aspects of schizophrenia (Lipska 2004; Lipska & Weinberger 1993; Weinberger 1995).

Schizophrenia is a chronic, debilitating neuropsychological disease characterized by positive symptoms such as auditory hallucinations, delusions and disorganized thoughts; negative symptoms such as the flat effect, decreased motivation and decreased social interaction; and cognitive impairment (Lewis & Gonzalez-Burgos 2006). Glutamatergic dysfunction is hypothesized to be one of the major mechanisms of schizophrenia pathogenesis. Previously, we have performed systematic association studies of glutamate receptor genes with schizophrenia (Fukumaki & Shibata 2003) and found one susceptibility locus for schizophrenia located within or very close to the human GluR4 gene (*GRIA4*) in the Japanese population (Makino *et al.* 2003). To examine the role of the GluR4 subunit in the higher brain function and in pathophysiology of schizophrenia, we generated GluR4 knockout mice and conducted an electrophysiological test of hippocampus slices and the comprehensive behavioural test battery.

Materials and methods

Generation of GluR4 knockout mice

A genomic clone containing exon 12, which encodes the first transmembrane domains (M1) and the pore loop domain (M2)

doi: 10.1111/j.1601-183X.2010.00629.x

of GluR4, was isolated from a 129/SvJ mouse genomic library (Stratagene), and a 7.2-kb *Xba*I fragment 3′ to exon 12 was subcloned. A 1.7-kb fragment 5′ to exon 12 was obtained by polymerase chain reaction (PCR). The targeting vector used to generate the GluR4 knockout mice was constructed by replacing exon 12 with a *polII-neo*-poly(A) cassette and flanking the cassette with a pair of herpes simplex virus thymidine kinase genes for negative selection (Tsuzuki *et al.* 2001). CCE embryonic stem cells (strain 129/SvJ) used in the previous study by Gondo *et al.* (1994) were electroporated with the targeting vector and selected in the medium containing G418 (250 μg/ml) and ganciclovir (5 μM). Double-resistant clones were subjected to Southern blot analysis to ensure the desired structure had been produced by the homologous recombination event. For the 0.5-kb 3′-flanking probe, the genomic DNA was cleaved with *Spe*I and the expected sizes of the hybridized bands for the wild-type and the mutant GluR4 alleles were 19.7 and 12.2 kb, respectively. For the 0.6-kb 5′-flanking probe, the DNA was digested with *Sph*I and the wild-type and mutant alleles produced 13.4 and 7.0 kb fragments, respectively. Five targeted ES clones were independently injected into C57BL/6J blastocysts and four of them yielded chimeric mice capable of transmitting the targeted GluR4 allele through the germ line. The mice carrying the mutated GluR4 allele were backcrossed to C57BL/6J for at least seven generations before behavioural analyses. Genotypes were determined by PCR analysis of tail genomic DNA. Two pairs of primers were used to detect wild-type and mutant alleles: a pair consisting of 5′-GCTACCACAAAAGATGGATGC-3′ as the forward primer and 5′-GGTTTTAGAATCCCCACAGCA-3′ as the reverse primer for the wild-type allele, and another pair consisting of 5′-AGGGACTGGCTGCTATTGG-3′ as the forward *neo* primer and 5′-GATGTTTCGCTTGGTGGTC-3′ as the reverse *neo* primer for the mutated allele.

Western blot analysis

Mouse brains were dissected into cerebellum, cerebrum and hippocampus sections. Each specimen was sonicated five times using a BIORUPTOR (Cosmo Bio, Tokyo Japan) for 1 min at 30 second intervals in sodium dodecyl sulphate (SDS) buffer [2% SDS, 2 mM ethylenediaminetetraacetic acid, 50 mM Tris–HCl (pH 6.8) and 2 mM phenylmethylsulphonyl fluoride]. The proteins produced were assayed by the modified Lowry procedure and equal amounts (6–40 μg) of sample proteins were subjected to 8% SDS–polyacrylamide gel electrophoresis and electrophoretically transferred onto a PVDF membrane (Immobilon Membrane, MILLIPORE, Billerica, MA, USA). The blots were blocked with 5% non-fat dried milk and 0.1% Tween 20 in 0.01 M phosphate-buffered saline (PBS) for 1 h and then incubated with rabbit anti-GluR4 antibody (CHEMICON international, Inc., Temecula, CA, USA) for 1–2 h. After being rinsed in PBS twice for 10 min each, the membranes were incubated with horseradish peroxidase-conjugated goat anti-rabbit IgG diluted in PBS containing 0.1% Tween 20 for 1 h and washed with PBS three times for 10 min each. Then, the proteins were visualized by the enhanced chemiluminescence (Amersham Biosciences, Buckinghamshire, UK) method for detection.

Immunohistochemical analysis

The animals were deeply anesthetized with pentobarbital (90 mg/kg, i.p.). Then, they were immediately perfused with PBS (0.01 M) followed by 4% PFA (paraformaldehyde in PBS) and then had their brains removed, cut coronally into appropriate thick blocks and postfixed in 4% PFA overnight at 4°C. Four percentage of PFA was replaced with 30% sucrose in PBS, and the brain tissues were left overnight at 4°C. The tissues were embedded in optimal cutting temperature (OCT) compound (Tissue-Tek, Tokyo, Japan), snap frozen in isopentane and stored at −80°C until cryostat sectioning. Serial cryostat sections obtained from the cerebrum and the cerebellum in the coronal planes were cut and affixed to Super Micro Slide Glasses (Matsunami Glass Ind., Ltd., Osaka, Japan) at a cabinet temperature of −25°C. Before use, the sections were air dried for 30–60 min and incubated overnight at −80°C. After being thawed at room temperature, the cryostat sections were rinsed with PBS, incubated for 30 min in 0.3% H_2O_2 in PBS, washed with PBS and blocked for 1 h with blocking buffer (PBS containing 4% normal goat serum, 0.1% Triton-100X and 0.05% Tween 20). After being blocked, the cryostat sections were incubated overnight in a humidified chamber at 4°C with the primary antibodies, such as rabbit anti-GluR1 antibody, rabbit anti-GluR2 antibody and rabbit anti-GluR4 antibody (Chemicon) diluted in PBS. Then, the sections were rinsed repeatedly with PBS, blocked for 10 min and incubated for 1 h with biotinylated secondary antibody in blocking buffer. After being washed with PBS, the sections were then incubated with ABC Elite reagent containing horseradish peroxidase-avidin complex (Vector Laboratories, Burlingame, CA, USA) for 30 min and then washed with PBS again. The peroxidase reaction was performed using diaminobenzidine (DAB, Vector Laboratories) for 5 min. Finally, the sections were analysed with the Stemi 2000-C stereo microscope (ZEISS, Oberkochen, Germany). Images were acquired with the Axio Cam (ZEISS) and processed by Axio Vision 3.1 (ZEISS) and PHOTOSHOP software (Adobe, San Jose, CA, USA). The secondary antibody alone did not show any staining.

Electrophysiological analysis

Electrophysiological analyses were performed as reported previously (Ito *et al.* 2000; Kawakami *et al.* 2003) with 9-week-old mice. Mouse brains were removed after ether anesthesia and decapitation. Transverse hippocampal slices were cut with a vibrating microtome (VT 1000 S) in ice-cold NR (normal Ringer's solution saturated with 95% O_2/5% CO_2) and were incubated in NR to allow them to recover for at least 1 h at room temperature. All recordings were carried in a submerged slice chamber perfused with NR at 32 ± 0.5°C. A recording electrode filled with 0.9% NaCl was used for recording. Synaptic responses were evoked at 0.1 Hz using a bipolar tungsten electrode. Paired-pulse facilitation (PPF) was examined at 50 msecond interstimulus intervals with three traces. PPF values were calculated as the ratio of the second stimulus-evoked field excitory postsynaptic potential (fEPSP) peak divided by the first stimulus-evoked fEPSP peak. The tetanic stimuli used to evoke LTP consisted of two trains of 100 Hz stimuli lasting for 1 second at an intertrain interval of 10 seconds. The LTP of the fEPSP slope was expressed as the percentage of the mean before tetanic stimulation. To preclude bias, the PPF and LTP measurements were performed blind to genotypes. All data are expressed as a mean ± SEM and were analysed with the Student's *t*-test.

Behavioural analysis

A behavioural test battery was conducted as described previously (Yamasaki *et al.* 2008). The mutant mice were backcrossed to the C57BL/6J background for at least seven generations. GluR4$^{-/-}$ and GluR4$^{+/+}$ mice were generated by intercrossing males and females heterozygous for GluR4$^{+/-}$. We prepared one batch of mice for behavioural tests; the batch consisted of the same number of GluR4$^{-/-}$ and control mice ($n = 16$ and 16, respectively). All behavioural tests were carried out with male mice that were 10 weeks old at the start of the testing. The animals were housed four per cage in a room with a 12-h light–dark cycle (light on at 0800 h) and allowed *ad libitum* access to food and water. All behavioural tests were performed between 0900 h and 1900 h, except for the eight-arm radial maze test, which was performed between 2100 h and 0700 h. Before testing each animal, the apparatus was cleaned with diluted sodium hypochlorite solution to prevent bias because of olfactory cues. The experimenter remained blind to genotype during behavioural testing and mice were identified by ear punching. The raw data of behavioural tests, which are not described in this article, are disclosed in the gene-brain-phenotyping database (http://www.mouse-phenotype.org/).

General health and neurological screen

The ear twitch, whisker twitch, righting reflex and response to key jangling were evaluated. A number of physical features, including the presence of whiskers and bald patches, were also recorded. Neuromuscular strength and balance were examined with the grip strength test and the wire hang test. A grip strength metre was used to assess

forelimb grip strength when the mice were pulled back. In the wire hang test, a mouse was placed on a wire cage lid and then the lid was inverted and held at a height of approximately 30 cm above the cage litter. Latency to fall was recorded, with a 60 second cutoff time.

Open-field test

Locomotor activity was measured using an open-field test. Each subject was placed in the centre of the open-field apparatus, which was illuminated (100 lux). The apparatus was cleaned with water after each trial. Motor activity parameters (distance travelled, number of vertical and stereotypical movements and centre time) were then monitored and recorded over a 120-min period.

Barnes maze test

The Barnes maze task was conducted on 'dry land', a white circular surface, 1.0 m in diameter, with 12 holes equally spaced around the perimeter (O'Hara & Co., Tokyo, Japan). A black Plexiglass escape box (17 × 13 × 7 cm), which had paper cage bedding on its bottom, was located under one of the holes. The hole above the escape box represented the target, analogous to the hidden platform in the Morris task. The location of the target was consistent for a given mouse but randomized across mice. The maze was rotated daily, with the spatial location of the target unchanged with respect to the distal visual room cues, to prevent a bias based on olfactory or the proximal cues within the maze. The mice that could not find the tunnel were guided to it and allowed to remain there for 1 min. Two trials per day were conducted for 10 successive days. Each trial ended when the mouse entered the goal tunnel or after 5 min had elapsed. The amount of time that the mice took to enter the tunnel (escape latency) and the number of errors (defined by the animal placing its nose in a hole that did not lead to the escape chamber) were recorded by IMAGE BM software for each trial. On day 11, a probe test was conducted without the escape box, to confirm that this spatial task had been performed based on navigation using distal environment room cues. Another probe trial was conducted 10 days after the last training session to evaluate memory retention. The time spent around the target hole was recorded in these probe tests by the software.

Startle response/prepulse inhibition test

The response to being acoustically startled and prepulse inhibition (PPI) of the acoustic startle response were measured using a startle reflex measurement system. The test session began by placing a mouse in a Plexiglass cylinder and leaving the mouse undisturbed for 10 min. The startle stimulus was white noise played for 40 mseconds at 110 or 120 dB, and the background noise level was 70 dB. The prepulse sound was presented 100 mseconds before the startle stimulus, for 40 mseconds, and its intensity was 74 or 78 dB. The background noise level in each chamber was 70 dB. The peak startle amplitude recorded during the 140 msecond sampling window was used as the dependent variable. A test session consisted of six trial types (i.e. two types for startle-stimulus-only trials and four types for PPI trials). Four combinations of prepulse and startle stimuli were used (74/110, 78/110, 74/120 and 78/120 dB). Six blocks of six different trial types (four trial types with the combination of prepulse and startle stimulus and two startle-stimulus-only trials) were presented in a pseudorandom order such that each trial type was presented once within a block. The mean intertrial interval was 15 seconds (range 10–20 seconds). The startle amplitude (I_{max}) was also determined. After the test, mean values of I_{max} were calculated for the six trial types. The percentage PPI was defined as [{I_{max} (startle stimulus)} - {I_{max} (prepulse and startle stimulus)}]/I_{max} (startle stimulus) × 100.

Sensitivity to MK-801

To test the locomotor-activating effects of MK-801, the mice were habituated to an open field for 1 h and then MK-801 was administered i.p. at 0.25 mg per 1 kg of body weight after being dissolved in saline. A dose of 0.2 mg/kg MK-801 is sufficient to observe the locomotor hyperactivity-inducing effect on mice (Karlsson *et al.* 2008). As there was a difference in baseline locomotor activity between genotypes, the ratio of activity during the hour after injection to the activity during the hour before injection was used as an index of the locomotor-activating effects of the drug.

T-maze test

The forced alternation test was conducted as previously described (Takao *et al.* 2008). The maze was constructed of white plastics runways with walls 25-cm high and partitioned into the right and left arms (11.5 × 20.5 cm) and the stem (13 × 24 cm) area by automated sliding doors. The end of each arm was equipped with a food dispenser that was able to provide a food reward. The pellet sensors were able to automatically record the pellet intake by the mice. After making their arm choice, the mice were able to return to the starting compartment, namely the stem of the T-maze, through a runway. A variety of fixed extra-maze clues surrounded the apparatus. The mice were kept on a maintenance diet as described above. After dieting, all mice underwent 3 days of habituation to the apparatus and received rewards (10-min of exposure to the maze each day, with rewards placed at both ends of the T-maze). On the first (sample) run of each trial, both goal arms were baited, but the mouse was forced to choose one of the goal arms (the other being blocked by a removable door). After entering the preselected goal arm, the mouse was allowed 20 seconds to consume the reward and then could go back to the start box. During the second run (choice), both goal arms were open and the mouse was rewarded for choosing the previously unvisited arm. The location of the sample arm (left or right) was varied pseudorandomly across trials so that the mice received equal numbers of left and right presentations, but no more than two consecutive trials had the same sample location. These daily training sessions were continued for 11 days, with 10 trials performed per day. To set higher demands on working memory, intratrial intervals between two runs (sample and choice) were set at 10, 30 and 60 seconds. Next, the mice were tested for Left–Right discrimination in the T-maze (Ikeda *et al.* 2008). The mice were placed in the stem of the T-maze. The door leading to the straight alley was opened and the mice were able to freely choose either the right or left arm of the T-maze. If a mouse chose the baited (correct) arm, it was allowed to consume the food reward. The mouse was then allowed to return to the starting compartment. The correct arm was assigned to each mouse randomly. On day 7, the correct arm was changed to test reversal learning.

Image and statistical analyses

The applications used for the behavioural studies were IMAGE LD, IMAGE EP, IMAGE RM, IMAGE FZ and IMAGE SI, which were written by T. Miyakawa based on the public domain NIH Image programme (developed at the US National Institutes of Health and available on the Internet at http://rsb.info.nih.gov/nih-image/) and the ImageJ programme (http://rab.info.nih.gov/ij/), which was modified for each test by T. Miyakawa (available through O'Hara & Co.). Statistical analysis was conducted using Excel (Microsoft, Redmond, WA, USA) and STATVIEW (SAS institute, Cray, NC, USA). Data were analysed using the two-tailed *t*-test, one-way ANOVA, two-way ANOVA or repeated-measures ANOVA and are presented as mean ± SEM.

Result

Generation of GluR4 knockout mice

To disrupt the GluR4 locus, an isogenic targeting vector was designed to delete the M1 and the M2 domains, which are encoded by exon 12 and are essential for the function of the receptor (Fig. 1a). Targeted disruption of the GluR4 gene was confirmed by Southern hybridization of tail genomic DNA (Fig. 1b). Western blot analysis of the brain specimens with the antibody against the C-terminal domain of GluR4 showed no detectable GluR4 protein in the GluR4$^{-/-}$ mouse and reduced expression in the GluR4$^{+/-}$ mouse (Fig. 1c).

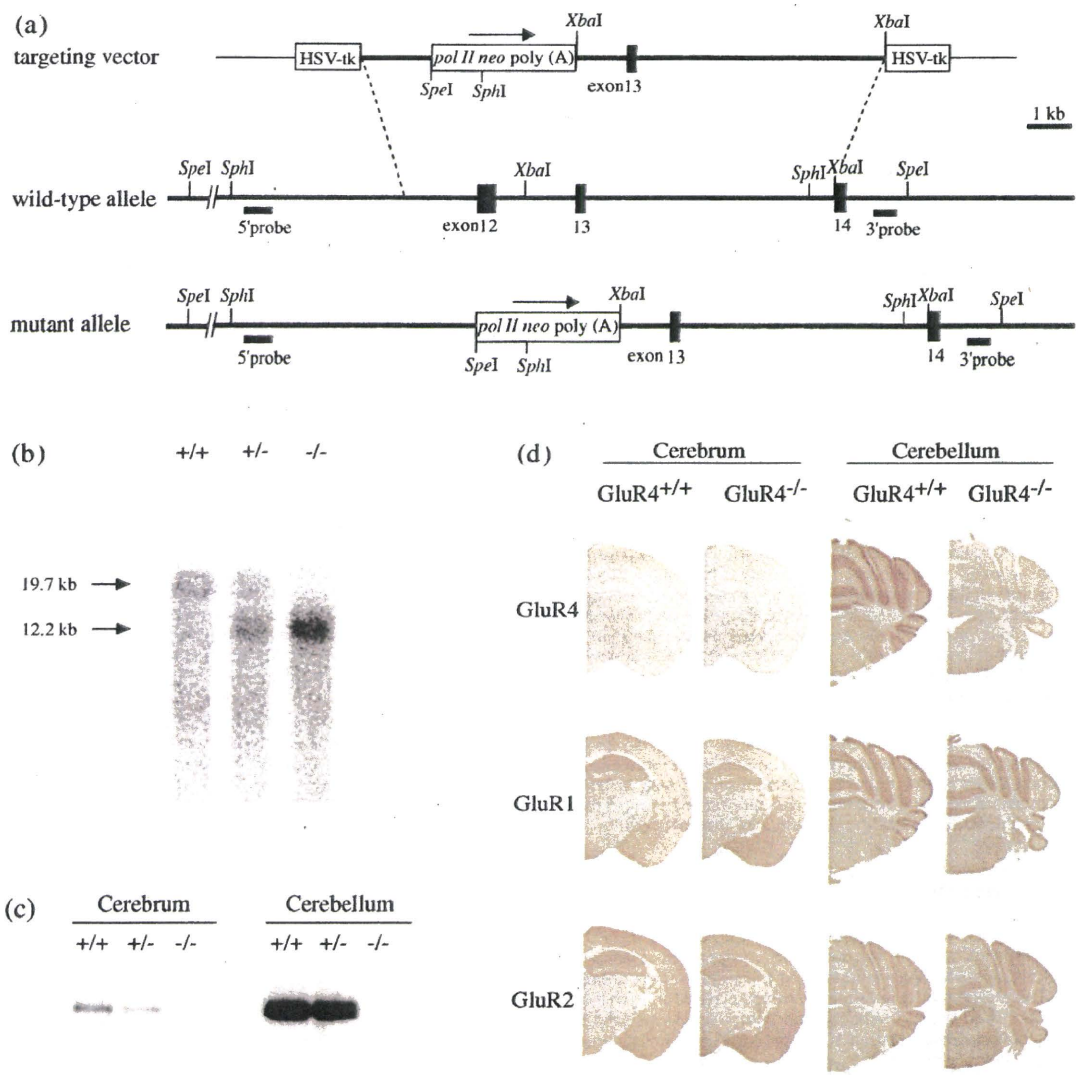

Figure 1: Targeted disruption of the GluR4 gene in the mouse. (a) Targeting of the GluR4 gene. The upper line represents the targeting vector, the middle line represents the wild-type GluR4 gene allele and the lower line shows the mutated GluR4 gene allele. The thick lines show genomic sequences with exons (filled square), whereas the thin lines show the bacterial plasmid portion. Open squares represent a positive [*polII-neo*-poly (A)] and a negative (HSV-tk) selection cassette. The positions of the 5′-flanking and 3′-flanking probes for Southern blot analysis are indicated. (b) Southern blot analysis of genomic DNA from mice. The DNA was cleaved with *SpeI* and probed with the external 3′-flanking probe. Restriction fragments of 19.7 kb from the wild-type allele and 12.2 kb from the mutant allele were observed. (c) Western blot analysis of GluR4 subunit protein in the mice of each genotype. (d) Immunostaining of AMPA receptor subunits (GluR4, GluR1 and GluR2) in cerebral and cerebellar sections of the mouse with each genotype.

Immunohistochemical analysis of other AMPA receptor subunits (GluR1 and GluR2) in the cerebral and cerebellar sections of the GluR4$^{-/-}$ mice brain showed that there was no gross anatomical change in the hippocampus, neocortex or cerebellar cortex of the GluR4$^{-/-}$ mice brain, and no abnormal distribution of GluR1 or GluR2 was seen in any layer of the GluR4$^{-/-}$ mouse brain sections (Fig. 1d).

Electrophysiological properties of GluR4$^{-/-}$ mice

GluR4 is a subunit of the AMPA receptors, which are important for the expression of several forms of long-lasting synaptic plasticity including LTP and LTD (Bear & Abraham 1996; Bliss & Collingridge 1993; Malenka & Nicoll 1999). We investigated short- and long-term synaptic plasticity by assessing the paired-pulse ratio (PPR) and LTP, respectively,

in the CA1 region of the 9-week-old mouse hippocampus (Fig. 2). We observed PPF in GluR4$^{-/-}$ and GluR4$^{+/+}$ mice, but detected no differences in the amplitude of PPF between the two genotypes (Fig. 2a). Regarding LTP, the EPSP slope at 60 min after tetanus was normalized using the mean slope before stimulation. There were no statistically significant differences in the LTP between two genotypes (Fig. 2b), suggesting that GluR4 is not essential for LTP in the CA1 region of the hippocampus of 9-week-old mice.

General characteristics and anxiety-related behaviour of GluR4$^{-/-}$ mice

A behavioural test battery was conducted as described previously (Yamasaki *et al.* 2008). We used male GluR4$^{-/-}$ mice ($n = 16$), which were backcrossed to the C57BL/6J background for at least seven generations, and their 10-week-old male GluR4$^{+/+}$ littermates ($n = 16$). The mutant mice had a normal body temperature (Fig. 3a) and showed no obvious abnormalities on gross inspection of their fur, whiskers and posture. The GluR4$^{-/-}$ mice weighed approximately 10% less than their wild-type littermates [Fig. 3b; two-tailed *t*-test, $t(30) = 3.030$, $P = 0.0050$, $n = 16$ each]. Casual trials of righting reflex, whisker touch reflex, ear twitch reflex and the response to key jangling were normal in all of the mice. The results of the tests are open to the public in the gene-brain-phenotyping database (http://www.mouse-phenotype. org/).

The grip strength test showed a muscle weakness of the GluR4$^{-/-}$ mice compared with GluR4$^{+/+}$ mice [Fig. 3d; two-tailed *t*-test, $t(30) = 2.920$, $P = 0.0066$, $n = 16$ each]. In the wire hang test, however, there was no difference in the latency until falling between GluR4$^{-/-}$ and GluR4$^{+/+}$ mice (Fig. 3c). This may be because of the low body weight of GluR4$^{-/-}$ mice.

In the open-field test, no significant difference was observed in the distance travelled and the stereotypic counts between GluR4$^{-/-}$ and GluR4$^{+/+}$ mice (Fig. 4a,d). The vertical activity was reduced in the GluR4$^{-/-}$ mice compared with the controls [Fig. 4b; two-way repeated-measures ANOVA, $F(1,30) = 9.902$, $P = 0.0037$, $n = 16$ each]. We also examined the response to a novel environment of the mice in the open-field test (Fig. 4c). There was no statistically significant difference between the two groups in the time spent in the central area, suggesting that the GluR4$^{-/-}$ mice showed a normal anxiety-like behaviour in a novel environment. To further examine anxiety-related behaviour of mutant mice, we performed the elevated plus maze test. Again, no significant differences between the GluR4$^{-/-}$ and GluR4$^{+/+}$ mice were found in any of the parameters examined (Fig. S1). Although, in the light–dark transition test, GluR4$^{-/-}$ and GluR4$^{+/+}$ mice ($n = 16$each) showed similar

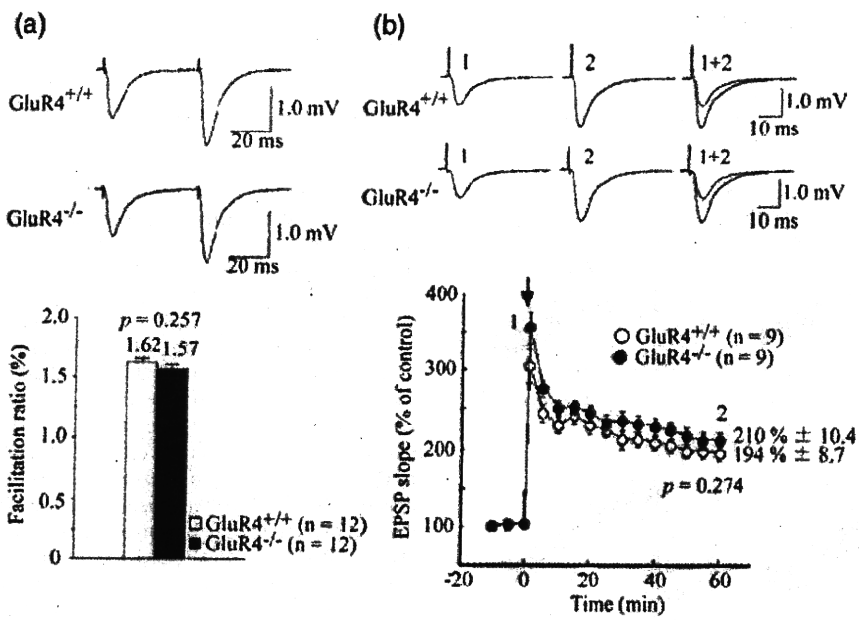

Figure 2: Electrophysiological analysis. (a) (top) Paired-pulse ratios assessed at 50 msecond intervals; scale: 1.0 mV, 20 mseconds. (bottom) PPR values were calculated as the ratio of the second stimulus-evoked fEPSP peak divided by the first stimulus-evoked fEPSP peak. Mean ratios from GluR4$^{+/+}$ (open bar) and GluR4$^{-/-}$ (filled bar) slices of the relevant mice ($n = 12$ each). (b) (top) Average traces recorded at times 1 and 2; scale: 1.0 mV, 10 mseconds. (bottom) The arrow indicates the time when the tetanic stimuli were applied. Regarding LTP, the normalized EPSP slope for the GluR4$^{+/+}$ mice at 60 min after tetanus was 194 ± 8.7% of the mean slope before stimulation and that for GluR4$^{-/-}$ mice was 210 ± 10.4%. Although there was a slight difference in the total time-course of EPSP slope in the GluR4$^{-/-}$ mice, no statistically significant difference was observed in the magnitude of LTP obtained from GluR4$^{+/+}$ and GluR4$^{-/-}$ slices ($n = 9$ each, $P = 0.274$). All data are expressed as mean ± SEM and were analysed with the Student's *t*-test.

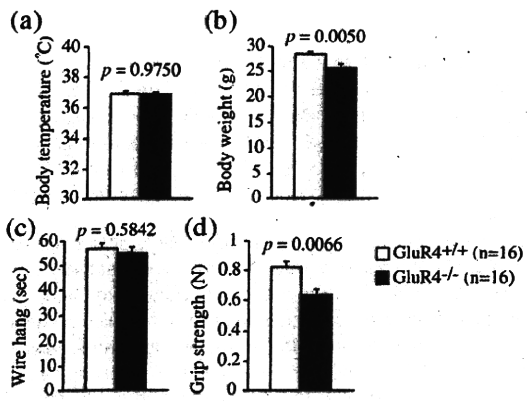

Figure 3: General health and neurological screening in GluR4$^{-/-}$ mice. (a) The GluR4$^{-/-}$ and GluR4$^{+/+}$ mice had similar body temperatures. (b) The GluR4$^{-/-}$ mice (filled bar) weighed approximately 10% less than the GluR4$^{+/+}$ mice (open bar) ($P = 0.0050$). (c) In the wire hang test, the latency until falling onto the bedding was similar in the GluR4$^{-/-}$ and GluR4$^{+/+}$ mice. (d) In the grip strength test, the GluR4$^{-/-}$ mice showed weaker muscular function of the forelimb ($P = 0.0066$).

total distance travelled (Fig. S2a) and similar total time spent in the lit compartment (Fig. S2b), the number of transitions was lower in GluR4$^{-/-}$ than GluR4$^{+/+}$ mice [Fig. S2c; two-way ANOVA, $F(1,30) = 15.975$, $P = 0.0004$, $n = 16$ each]. The latency to the first transition also tends to increase in GluR4$^{-/-}$ mice (Fig. S2d), indicating that GluR4$^{-/-}$ mice showed an increase in anxiety-like behaviour only against the light.

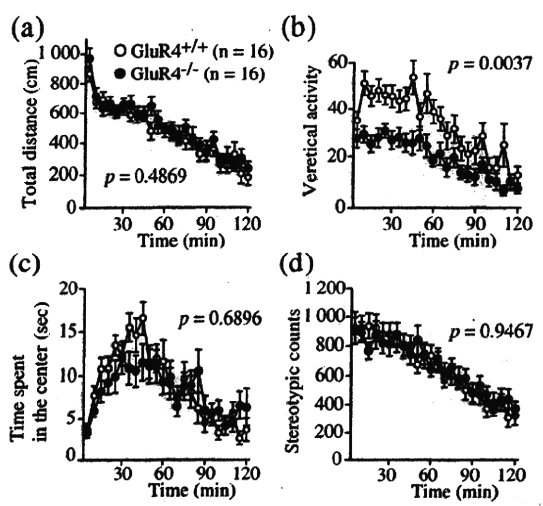

Figure 4: Locomotor activity of GluR4$^{-/-}$ mice in the open-field test. Time-course of distance travelled (a), vertical activity (b), time spent in the central area (c) and stereotypic counts (d) are shown ($n = 16$ each). The vertical activity was reduced in the GluR4$^{-/-}$ mice compared with the GluR4$^{+/+}$ mice (b, $P = 0.0037$). Data are represented as mean ± SEM.

Learning and memory skills of GluR4$^{-/-}$ mice

AMPA receptors are involved in learning and memory in the hippocampus through the activation of *N*-methyl-D-aspartate (NMDA) receptors. Therefore, it was intriguing to test whether spatial learning and memory functions were affected in the GluR4$^{-/-}$ mice. We examined the performance of GluR4$^{-/-}$ mice in the Barnes circular maze test, a hippocampus-dependent cognitive task that requires spatial reference memory. Both the GluR4$^{-/-}$ and GluR4$^{+/+}$ mice learned to locate the escape hole during the course of the training period (days 1–10), as indicated by a progressive reduction in their errors rates (errors were defined as visits to any non-target hole). In the training period, the GluR4$^{-/-}$ mice showed a significantly greater number of errors than the GluR4$^{+/+}$ mice [Fig. 5a; two-way repeated-measures ANOVA, $F(1,30) = 5.075$, $P = 0.0317$, $n = 16$ each]. In the first probe test conducted 1 day after the last training test, the GluR4$^{-/-}$ mice spent significantly less time around the target hole than the GluR4$^{+/+}$ mice [Fig. 5b; paired *t*-test, $t(30) = 2.133$, $P = 0.0412$, $n = 16$ each]. In the second probe test conducted 10 days after the last training test, the GluR4$^{-/-}$ and GluR4$^{+/+}$ mice ($n = 16$ each) performed equally well (Fig. 5c). These results suggest that the loss of GluR4 affected the acquisition of spatial reference memory, but not the consolidation/retention.

Schizophrenia-related characteristics of GluR4$^{-/-}$ mice

Prepulse inhibition of the acoustic startle response is an index of sensorimotor gating and is one of a few neuropsychological measures in which humans and rodents can be evaluated in a similar fashion, and impairment in PPI is a prominent feature of schizophrenia symptomatology (Braff & Geyer 1990). The startle response to acoustic stimulation at 110 and 120 dB in the GluR4$^{-/-}$ mice was smaller than that seen in the GluR4$^{+/+}$ mice [Fig. 6a; overall ANOVA including all four conditions, $F(1,30) = 7.937$, $P = 0.0085$, $n = 16$ each]. This could be because of the effects of low body weight and weakened muscle strength on the amplitude of whole body flinching. We cannot rule out a possibility of hearing deficit of GluR4 knockout mice. However, even if it exists, hearing ability of the mice might not be impaired severely, because of the fact that the startle response was observed at both sound levels 110 and 120 dB in the GluR4$^{-/-}$ mice. The intensity of the prepulse sound was 74 or 78 dB and four combinations of prepulse and startling stimuli were used (74/110, 78/110, 74/120 and 78/120 dB). The percentage PPI was significantly lower in the GluR4$^{-/-}$ mice than in the controls (Fig. 6b). The difference between genotypes was greater when the 74/110 and 78/110 dB combinations of prepulse/startle stimuli were used [overall ANOVA including all four conditions, $F(1,30) = 6.733$, $P = 0.0145$, $n = 16$ each], indicating that the GluR4$^{-/-}$ mice showed dramatically impaired PPI, a schizophrenia endophenotype. At the stimulus intensity of 120 dB, no significant difference between the genotypes

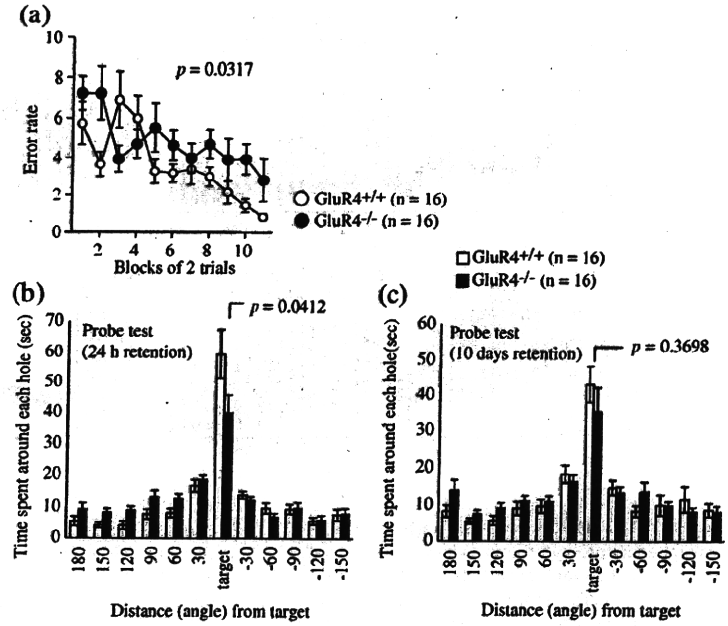

Figure 5: GluR4$^{-/-}$ mice in the Barnes maze. (a) Error rates. GluR4$^{-/-}$ mice made significantly more errors (defined as visits to any non-target hole) than the GluR4$^{+/+}$ mice ($P = 0.0317$, $n = 16$ each). The number of errors decreased across training days in both the GluR4$^{-/-}$ and GluR4$^{+/+}$ mice. (b) The probe test at one day after the last training day. The GluR4$^{-/-}$ mice spent significantly more time around the target hole than the GluR4$^{+/+}$ mice ($P = 0.0412$). (c) The probe test at 10 days after the last training day. There was no significant difference in the time spent around the target hole between the GluR4$^{-/-}$ and GluR4$^{+/+}$ mice. Values are given as mean ± SEM.

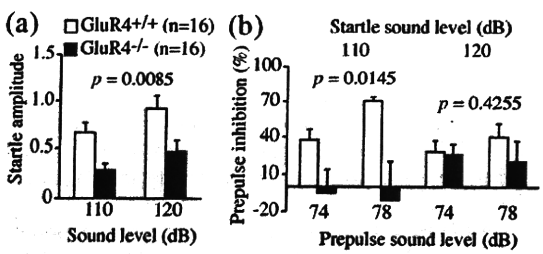

Figure 6: Startle response and the PPI in GluR4$^{-/-}$ mice. (a) Startle amplitude was significantly decreased in the GluR4$^{-/-}$ mice ($P = 0.0085$, $n = 16$ each). (b) The percentage PPI was significantly lower in the GluR4$^{-/-}$ mice compared with that in the controls when the startle stimulus intensity was 110 dB ($P = 0.0145$, $n = 16$ each). Data represent mean ± SEM.

was observed, probably because of a ceiling effect caused by the strong intensity of the startle stimulus.

Sensitivity to the NMDA receptor antagonist MK-801 is increased in schizophrenia patients (Lieberman *et al.* 1987). To investigate the effects of NMDA receptor antagonism in GluR4$^{-/-}$ mice, we assessed the locomotor stimulatory effects of MK-801. Interestingly, the peaks of the GluR4$^{-/-}$ mice in the total distance travelled [Fig. 7a; two-way repeated-measures ANOVA, genotype X time interaction, $F(16, 224) = 2.235$, $P = 0.0051$, $n = 8$ each] and the stereotypic counts [Fig. 7d; two-way repeated-measures ANOVA, genotype X time interaction, $F(16, 224) = 10.301$, $P < 0.0001$, $n = 8$ each] after treatment with MK-801 were seen 15 min sooner than in their controls. Although these results may only indicate a pharmacokinetic effect and do not represent classic increases in sensitivity to MK-801 of GluR4$^{-/-}$ mice, the data conceivably suggest that GluR4$^{-/-}$ mice have a higher sensitivity to MK-801 as observed in patients with schizophrenia. The vertical activity of GluR4$^{-/-}$ mice was low before administration of MK-801 [Fig. 7b; two-way repeated-measures ANOVA, genotype X time interaction, $F(16, 224) = 3.734$, $P < 0.0001$, $n = 8$ each], corresponding to the results obtained from the open-field test (Fig. 4b). There was no significant difference between the mutant and control mice in the time spent in the central area (Fig. 7c).

We further examined other schizophrenia-related phenotypes in GluR4$^{-/-}$ mice: increased locomotor activity, decreased social behaviour and deficits in spatial working memory. There was no significant difference between the mutant and control mice in the distance travelled in the open-field test (Fig. 4a), indicating that the GluR4$^{-/-}$ mice exhibited normal spontaneous locomotor activity.

We also monitored the basal activity levels of the mice in a familiar environment. The activity of the GluR4$^{-/-}$ mice in the home-cage behavioural test was similar to that of the GluR4$^{+/+}$ mice (Fig. S3). Both the GluR4$^{-/-}$ and GluR4$^{+/+}$ mice had a characteristic circadian rhythm and showed a higher activity level during the dark phase of the cycle (Fig. S3a). Social interaction with a familiar cagemate in the home cage was similar between the GluR4$^{-/-}$ and GluR4$^{+/+}$ mice (Fig. S3b). The mean duration per contact was significantly increased in the GluR4$^{-/-}$ mice in the social interaction test [Fig. S4d; two-way ANOVA, $F(1, 13) = 6.086$, $P = 0.0283$, $n = 8$ (GluR4$^{+/+}$), 7 (GluR4$^{-/-}$) pairs] and the total duration of contact tends to increase in the GluR4$^{-/-}$ mice (Fig. S4a), suggesting that the social behaviour of the GluR4$^{-/-}$ mice was slightly improved.

To examine whether the lack of the GluR4 subunit was associated with changes in spatial working memory, which requires hippocampal function (Olton *et al.* 1978), the mice

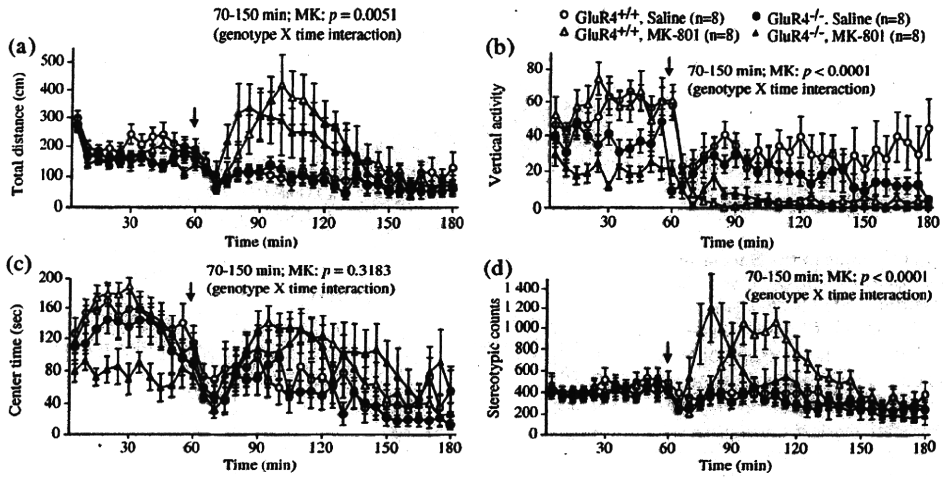

Figure 7: Locomotor-activating effects of MK-801. Time-course of distance travelled (a), vertical activity (b), time spent in the central area (c) and stereotypic counts (d) were shown [GluR4$^{-/-}$ mice with saline (filled circles), GluR4$^{-/-}$ mice with MK-801 (filled triangles), GluR4$^{+/+}$ mice with saline (open circles) and controls with MK-801 (open triangles), $n = 8$ each]. The arrows indicate the time when MK-801 was administered i.p. (0.25 mg/kg) ($t = 60$ min). The locomotor stimulatory effect of MK-801 was significantly faster in the GluR4$^{-/-}$ mice compared with that in the controls (a, $P = 0.0051$; d, $P < 0.0001$).

were subjected to the T-maze and eight-arm radial maze tests. The T-maze experiments were performed with food-restricted mice, using food pellets placed at the ends of the two arms of the T-maze. The mice were subjected to daily training sessions consisting of 10 consecutive test trials in which the mice had to remember the location of the previously visited arm to obtain a food reward. During the 11-day training period, the GluR4$^{-/-}$ and GluR4$^{+/+}$ mice gradually improved their performance (Fig. 8a). Interestingly, the GluR4$^{-/-}$ mice showed significantly higher performance in the number of correct choices made throughout the training period than the GluR4$^{+/+}$ mice [Fig. 8a; two-way repeated-measures ANOVA, $F(1,30) = 4.918$, $P = 0.0343$, $n = 16$ each]. However, when using 10, 30 and 60 second delays as intratrial intervals, the two groups did not differ significantly in their number of correct choices (Fig. 8b), indicating that the GluR4$^{-/-}$ mice showed improved spatial working memory only in the task with no delay. We then performed the Left–Right discrimination test in the T-maze. In the first 6 days, in which the baited arm was fixed to one side, both the GluR4$^{-/-}$ and GluR4$^{+/+}$ mice showed similar laterality (Fig. 8c). After day 7, the baited arm was changed and the number of correct choices was significantly higher in the GluR4$^{-/-}$ than the GluR4$^{+/+}$ mice [Fig. 8c; two-way repeated-measures ANOVA, $F(1,30) = 5.540$, $P = 0.0253$, $n = 16$ each]. This result indicates that GluR4$^{-/-}$ mice have a weaker perseveration tendency and higher behavioural flexibility than their controls. We then tested these animals with the eight-arm radial maze test and observed no significant difference in learning or memory performances between the GluR4$^{-/-}$ and GluR4$^{+/+}$ mice (Fig. S5). The results obtained from the T-maze and the eight-arm radial maze tests indicate that the lack of the GluR4 subunit mildly improves the spatial working memory.

Discussion

In this study, we subjected GluR4-deficient mice to a comprehensive behavioural test battery and showed that they exhibited schizophrenia-related phenotypes: drastically impaired PPI of the acoustic startle response and enhanced sensitivity to the locomotor stimulatory effects of a NMDA receptor antagonist, MK-801.

PPI of the acoustic startle reflex is a measure of sensorimotor gating, a pre-attentional inhibitory brain mechanism to filtrate extraneous stimuli from the outside (Geyer *et al.* 2001). The impaired PPI has been reported in individuals with a range of psychiatric and neurological disorders and most evidence was observed in schizophrenia (Braff *et al.* 2001). PPI can be tested in a similar fashion in humans and rodents. As a reproducible phenotypic marker, impaired PPI is regarded as a neurophysiological endophenotype of schizophrenia (Turetsky *et al.* 2007). For this reason, it has been widely used to study the neurobiology of schizophrenia and the effects of medications against it (Dawson *et al.* 2000; Ellenbroek *et al.* 1995; Geyer *et al.* 2001, 2002; Swerdlow *et al.* 2000). Many reports have shown that phencyclidine and other non-competitive NMDA receptors antagonists, such as dizocilpine and ketamine, potently disrupt PPI (Geyer *et al.* 2001; Mansbach & Geyer 1989). Furthermore, it has been reported that mice lacking the GluR1 subunit of AMPA receptor (Wiedholz *et al.* 2008) and the group I metabotropic glutamate receptors (mGluR1 and mGluR5) exhibit PPI disruption (Brody & Geyer 2004; Brody *et al.* 2003, 2004). In this study, GluR4 knockout mice also showed strong PPI deficits (Fig. 6b), indicating that the glutamatergic dysfunction may contribute to the impairment of PPI. The GluR4 KO mice developed by Deltagen do not seem to show any PPI deficit, at least according to the information provided by the company

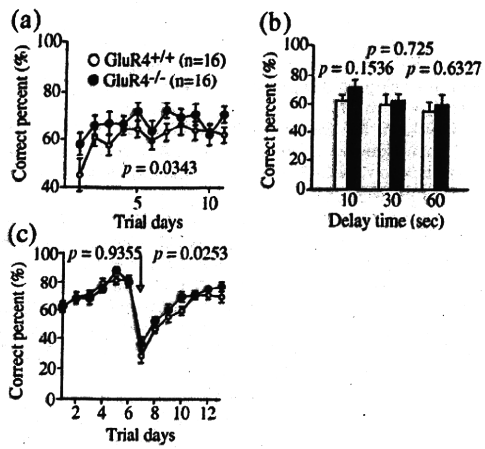

Figure 8: Performance in the T-maze test in GluR4$^{-/-}$ mice. T-maze experiments (spatial delayed alternation task) were performed as described in *Materials and Methods* section. (a) The GluR4$^{-/-}$ mice (filled circle) showed significantly higher performance in the number of correct choices than GluR4$^{+/+}$ mice (open circle) ($P = 0.0343$). (b) In contrast, in sessions with a 10, 30 or 60 seconds delay, the two groups did not differ significantly in the number of correct choices. Values represent the percentage of correct choices per session (maximum possible number of correct choices, 10). (c) Behavioural laterality and preservation tendency in the T-maze test. In the first 6 days, when the baited arm was fixed to one side, the GluR4$^{-/-}$ and GluR4$^{+/+}$ mice showed similar laterality. However, in the following 7 days as indicated by an arrow, when the baited arm was changed to the opposite side, the correct choice percentage was significantly higher in the GluR4$^{-/-}$ than the GluR4$^{+/+}$ mice ($P = 0.0253$). Data are given as mean ± SEM ($n = 16$each).

(http://www.informatics.jax.org/external/ko/deltagen/1624.html). This discrepancy might be because of difference in genetic backgrounds between the GluR4 knockout mice of Deltagen and of ours. The strain-dependent change in PPI was observed among inbred mouse strains (Pietropaolo & Crusio 2009).

Sensitivity to MK-801 is increased in individuals with schizophrenia (Lieberman *et al.* 1987) as well as in several mouse models of this condition: calcineurin knockout mice (Miyakawa *et al.* 2003), *Prodh*-knockdown mice (Paterlini *et al.* 2005) and NCAM-EC transgenic mice (Pillai-Nair *et al.* 2005). GluR4 knockout mice also showed increased sensitivity to the locomotor stimulatory effects of MK-801 (Fig. 7). In contrast to the observation, mice lacking GluR1, one of the major subunits of the AMPA receptor, showing impaired PPI did not exhibit a locomotor-stimulant response to MK-801 (Wiedholz *et al.* 2008). In this study, the results suggest that two behavioural abnormalities observed in GluR4-deficient mice may not be because of a secondary effect to functions of the GluR1 subunit in AMPA receptors.

Although GluR4 knockout mice exhibited two schizophrenia-related phenotypes: impaired PPI and high sensitivity to MK-801, the GluR4-deficient mice did not manifest other major schizophrenia-related phenotypes: increased locomotor activity, decreased social behaviour and impairment of spatial working memory. Glutamatergic dysfunction because of the loss of GluR4 leading to the schizophrenia endophenotypes is not sufficient to cause the behavioural abnormalities related to clinical symptoms, such as decreased social interaction, which may require additional genetic factors and/or environmental factors to establish schizophrenia phenotypes because of the multifactorial background of schizophrenia pathogenesis. In fact, according to the results from recent genome-wide association studies, there could be potentially thousands of very small individual effects that collectively account for a substantial proportion of variation in risk of schizophrenia (The International Schizophrenia Consortium 2009).

The GluR1-deficient mice showed locomotor hyperactivity during exposure to open field and in response to a novel object and disorganized social behaviours during a dyadic conspecific encounter. Either abnormality was not observed in GluR4-deficient mice. Open-field locomotor hyperactivity in GluR1-deficient mice was normalized by treatment with the dopamine (DA) antagonist and neuroleptic haloperidol. Retarded clearance of DA was inferred by *in vivo* chronoamperometric measurement of extracellular DA clearance in the striatum of GluR1-deficient mice (Wiedholz *et al.* 2008). The absence of some schizophrenia-related behavioural abnormalities such as locomotor hyperactivity in GluR4-deficient mice might be because of loss of dysfunction of the DA circuit. Further studies addressing extracellular DA clearance in GluR4-deficient mice are needed.

In early postnatal development of the hippocampus, GluR4-containing AMPA receptors are initially selectively delivered to synapses and are subsequently exchanged with GluR2-containing AMPA receptors (Zhu *et al.* 2000). The GluR2 subunit plays a crucial role in determining the Ca^{2+}-impermeability of AMPA receptor complexes and is involved in the expression of LTP (Tanaka *et al.* 2000). In fact, GluR2-deficient mice showed enhanced LTP in the CA1 region of the hippocampus (Jia *et al.* 1996). We therefore expected that GluR4-deficient mice might present some abnormalities in synaptic plasticity or development of the functional neural circuitry in the hippocampus. However, there was no striking difference in the magnitude of LTP (Fig. 2b) and in the distribution of GluR2 in the hippocampus (Fig. 1d) between the GluR4-deficient and wild-type mice. Therefore, GluR2 recruitment in the early stage of development may be accomplished with other substitute molecules in GluR4 knockout mice.

Recently, Beyer *et al.* (2008) found that a major susceptibility locus for absence epilepsy (*spkw1*) is associated with *Gria4*. The GluR4 knockout mice developed by Deltagen showed frequent spike-wave discharges (SWD), characteristic of absence epilepsy. We have not examined the SWD of our GluR4-deficient mice, because we have no apparatus available for the electroencephalogram analysis.

Interestingly, mild improvement of spatial working memory was observed in GluR4-deficient mice in the T-maze test (Fig. 8a). The retention of spatial reference memory was intact in the mutant mice, while the acquisition of spatial reference memory was impaired in the Barnes circular maze test (Fig. 5a). These observations suggest that GluR4 may

be involved in both working and reference memories. In GluR1-deficient mice impaired spatial working memory and intact spatial reference memory were reported (Schmitt *et al.* 2004; Zamanillo *et al.* 1999). The mice lacking GluR1 have deficits in hippocampal CA3-CA1 LTP (Zamanillo *et al.* 1999), suggesting the involvement of LTP in spatial working memory. However, there was no statistically significant difference in the LTP observed in the electrophysiological test of the hippocampus of GluR4-deficient mice (Fig. 2b). Improved spatial working memory and no alteration in the LTP in the GluR4 knockout mice might be because of compensatory mechanisms for other glutamate receptor subunits in the GluR4 knockout mice, although no abnormal distribution of GluR1 was observed in the hippocampus of the knockout mice.

Further evaluation of the molecular and physiological properties of GluR4-deficient mice could provide new insights into psychiatric disorders with which patients show PPI impairments and functions of GluR4 in the cognitive system as well.

References

Bear, M.F. & Abraham, W.C. (1996) Long-term depression in the hippocampus. *Annu Rev Neurosci* **19**, 437–462.

Beyer, B., Deleuze, C., Letts, V.A., Mahaffey, C.L., Boumil, R.M., Lew, T.A., Huguenard, J.R. & Frankel, W.M. (2008) Absence seizure in C3H/HeJ and knockout mice caused by mutation of the AMPA receptor subunit *Gria4*. *Hum Mol Genet* **17**, 1738–1749.

Bliss, T.V.P. & Collingridge, G.L. (1993) A synaptic model of memory: long-term potentiation in the hippocampus. *Nature* **361**, 31–39.

Braff, D.L. & Geyer, M.A. (1990) Sensorimotor gating and schizophrenia. Human and animal model studies. *Arch Gen Psychiatry* **48**, 379–380.

Braff, D.L., Geyer, M.A. & Swerdlow, N.R. (2001) Human studies of prepulse inhibition of startle: normal subjects, patient groups, and pharmacological studies. *Psychopharmacology* **156**, 234–258.

Brody, S.A. & Geyer, M.A. (2004) Interactions of the mGluR5 gene with breeding and maternal factors on startle and prepulse inhibition in mice. *Neurotox Res* **6**, 79–90.

Brody, S.A., Conquet, F. & Geyer, M.A. (2003) Disruption of prepulse inhibition in mice lacking mGluR1. *Eur J Neurosci* **18**, 3361–3366.

Brody, S.A., Dulawa, S.C., Conquet, F. & Geyer, M.A. (2004) Assessment of a prepulse inhibition deficit in a mutant mouse lacking mGluR5 receptors. *Mol Psychiatry* **9**, 35–41.

Dawson, M.E., Schell, A.M., Hazlett, E.A., Nuechterlein, K.H. & Filion, D.L. (2000) On the clinical and cognitive meaning of impaired sensorimotor gating in schizophrenia. *Psychiatry Res* **96**, 187–197.

Ellenbroek, B.A., Geyer, M.A. & Cools, A.R. (1995) The behavior of APO-SUS rats in animal models with construct validity for schizophrenia. *J Neurosci* **15**, 7604–7611.

Fukumaki, Y. & Shibata, H. (2003) Glutamate receptor genes as candidates for schizophrenia susceptibility. *Drug Dev Res* **60**, 137–151.

Geyer, M.A., Krebs-Thomson, K., Braff, D.L. & Swerdlow, N.R. (2001) Pharmacological studies of prepulse inhibition models of sensorimotor gating deficits in schizophrenia: a decade in review. *Psychopharmacology (Berl)* **156**, 117–154.

Geyer, M.A., McIlwain, K.L. & Paylor, R. (2002) Mouse genetic models for prepulse inhibition: an early review. *Mol Psychiatry* **7**, 1039–1053.

Gondo, Y., Nakamura, K., Nakao, K., Sasaoka, T., Ito, K., Kimura, M. & Katsuki, M. (1994) Gene replacement of the p53 gene with the lacZ gene in mouse embryonic stem cells and mice by using two steps of homologous recombination. *Biochem Biophys Res Commun* **202**, 830–837.

Ikeda, M., Hikita, T., Taya, S., Uraguchi-Asaki, J., Toyo-oka, K., Wynshaw-Boris, A., Ujike, H., Inada, T., Takao, K., Miyakawa, T., Ozaki, N., Kaibuchi, K. & Iwata, N. (2008) Identification of YWHAE, a gene encoding 14-3-3epsilon, as a possible susceptibility gene for schizophrenia. *Hum Mol Genet* **17**, 3212–3222.

Ito, I., Kawakami, R., Sakimura, K., Mishina, M. & Sugiyama, H. (2000) Input-specific targeting of NMDA receptor subtypes at mouse hippocampal CA3 pyramidal neuron synapses. *Neuropharmacology* **39**, 943–951.

Jia, Z., Agopyan, N., Miu, P., Xiong, Z., Henderson, J., Gerlai, R., Taverna, F.A., Velumian, A., MacDonald, J., Carlen, P., Abramow-Newerly, W. & Roder, J. (1996) Enhanced LTP in mice deficient in the AMPA receptor GluR2. *Neuron* **17**, 945–956.

Karlsson, R.M., Tanaka, K., Heilig, M. & Holmes, A. (2008) Loss of glial glutamate and aspartate transporter (excitatory amino acid transporter 1) causes locomotor hyperactivity and exaggerated responses to psychotomimetics: rescue by haloperidol and metabotropic glutamate 2/3 agonist. *Biol Psychiatry* **64**, 810–814.

Kawakami, R., Shinohara, Y., Kato, Y., Sugiyama, H., Shigemoto, R. & Ito, I. (2003) Asymmetrical allocation of NMDA receptor epsilon2 subunits in hippocampal circuitry. *Science* **300**, 990–994.

Keinänen, K., Wisden, W., Sommer, B., Werner, P., Herb, A., Verdoorn, T.A., Sakmann, B. & Seeburg, P.H. (1990) A family of AMPA-selective glutamate receptors. *Science* **249**, 556–560.

Lewis, D.A. & Gonzalez-Burgos, G. (2006) Pathophysiologically based treatment interventions in schizophrenia. *Nat Med* **12**, 1016–1022.

Lieberman, J.A., Kane, J.M. & Alvir, J. (1987) Provocative tests with psychostimulant drugs in schizophrenia. *Psychopharmacology (Berl)* **91**, 415–433.

Lipska, B.K. (2004) Using animal models to test a neurodevelopmental hypothesis of schizophrenia. *J Psychiatry Neurosci* **29**, 282–286.

Lipska, B.K. & Weinberger, D.R. (1993) Delayed effects of neonatal hippocampal damage on haloperidol-induced catalepsy and apomorphine-induced stereotypic behaviors in the rat. *Brain Res Dev Brain Res* **75**, 213–22.

Makino, C., Fujii, Y., Kikuta, R., Hirata, N., Tani, A., Shibata, A., Ninomiya, H., Tashiro, N., Shibata, H. & Fukumaki, Y. (2003) Positive association of the AMPA receptor subunit GluR4 gene (*GRIA4*) haplotype with schizophrenia. *Am J Med Genet* **116B**, 17–22.

Malenka, R.C. & Nicoll, R.A. (1999) Long-term potentiation – a decade of progress?. *Science* **285**, 1870–1874.

Mano, I. & Teichberg, V.I. (1998) A tetrameric subunit stoichiometry for a glutamate receptor-channel complex. *Neuroreport* **9**, 327–331.

Mansbach, R.S. & Geyer, M.A. (1989) Effects of phencyclidine and phencyclidine biologs on sensorimotor gating in the rat. *Neuropsychopharmacology* **2**, 299–308.

Mansour, M., Nagarajan, N., Nehring, R.B., Clements, J.D. & Rosenmund, C. (2001) Heteromeric AMPA receptors assemble with a preferred subunit stoichiometry and spatial arrangement. *Neuron* **32**, 841–853.

Miyakawa, T., Leiter, L.M., Gerber, D.J., Gainetdinov, R.R., Sotnikova, T.D., Zeng, H., Caron, M.G. & Tonegawa, S. (2003) Conditional calcineurin knockout mice exhibit multiple abnormal behaviors related to schizophrenia. *Proc Natl Acad Sci USA* **100**, 8987–8992.

Olton, D.S., Walker, J.A. & Gage, F.H. (1978) Hippocampal connections and spatial discrimination. *Brain Res* **139**, 295–308.

Paterlini, M., Zakharenko, S.S., Lai, W.S., Qin, J., Zhang, H., Mukai, J., Westphal, K.G., Olivier, B., Sulzer, D., Pavlidis, P., Siegelbaum, S.A., Karayiorgou, M. & Gogos, J.A. (2005) Transcriptional and behavioral interaction between 22q11.2 orthologs modulates schizophrenia-related phenotypes in mice. *Nat Neurosci* **8**, 1586–1594.

Pietropaolo, S. & Crusio, W.E. (2009) Strain-dependent changes in acoustic startle response and its plasticity across adolescence in mice. *Behav Genet* **39**, 623–631.

Pillai-Nair, N., Panicker, A.K., Rodriguiz, R.M., Gilmore, K.L., Demyanenko, G.P., Huang, J.Z., Wetsel, W.C. & Maness, P.F. (2005) Neural cell adhesion molecule-secreting transgenic mice display abnormalities in GABAergic interneurons and alterations in behavior. *J Neurosci* **25**, 4659–4671.

Rosenmund, C., Stern-Bach, Y. & Stevens, C.F. (1998) The tetrameric structure of a glutamate receptor channel. *Science* **280**, 1596–1599.

Schmitt, W.B., Deacon, R.M., Reisel, D., Sprengel, R., Seeburg, P.H., Rawlins, J.N. & Bannerman, D.M. (2004) Spatial reference memory in GluR-A-deficient mice using a novel hippocampal-dependent paddling pool escape task. *Hippocampus* **14**, 216–223.

Swerdlow, N.R., Braff, D.L. & Geyer, M.A. (2000) Animal models of deficient sensorimotor gating: what we know, what we think we know, and what we hope to known soon. *Behav Pharmacol* **11**, 185–204.

Takao, K. & Miyakawa, T. (2006) Light/dark transition test for mice. *J Vis Exp* **1**, 104.

Takao, K., Toyama, K., Nakanishi, K., Hattori, S., Takamura, H., Takeda, M., Miyakawa, T. & Hashimoto, R. (2008) Impaired long-term memory retention and working memory in sdy mutant mice with a deletion in Dtnbp1, a susceptibility gene for schizophrenia. *Mol Brain* **1**, 11.

Tanaka, H., Grooms, S.Y., Bennett, M.V. & Zukin, R.S. (2000) The AMPAR subunit GluR2: still front and center-stage. *Brain Res* **886**, 190–207.

The International Schizophrenia Consortium, Purcell, S.M., Wray, N.R., Stone, J.L., Visscher, P.M., O'Donovan, M.C., Sullivan, P.F. & Sklar, P. (2009) Common polygenic variation contributes to risk of schizophrenia and bipolar disorder. *Nature* **460**, 748–752.

Tsuzuki, T., Egashira, A., Igarashi, H., Iwakuma, T., Nakatsuru, Y., Tominaga, Y., Kawate, H., Nakao, K., Nakamura, K., Ide, F., Kura, S., Nakabeppu, Y., Katsuki, M., Ishikawa, T. & Sekiguchi, M. (2001) Spontaneous tumorigenesis in mice defective in the MTH1 gene encoding 8-oxo-dGTPase. *Proc Natl Acad Sci USA* **98**, 11456–11461.

Turetsky, B.I., Calkins, M.E., Light, G.A., Olincy, A., Radant, A.D. & Swerdlow, N.R. (2007) Neurophysiological endophenotypes of schizophrenia: the viability of selected candidate measures. *Schizophr Bull* **33**, 69–94.

Weinberger, D.R. (1995) From neuropathology to neurodevelopment. *Lancet* **346**, 552–557.

Wiedholz, L.M., Owens, W.A., Horton, R.E., Feyder, M., Karlsson, R.M., Hefner, K., Sprengel, R., Celikel, T., Daws, L.C. & Holmes, A. (2008) Mice lacking the AMPA GluR1 receptor exhibit striatal hyperdopaminergia and 'schizophrenia-related' behaviors. *Mol Psychiatry* **13**, 631–640.

Yamasaki, N., Maekawa, M., Kobayashi, K. *et al.* (2008) Alpha-CaMKII deficiency causes immature dentate gyrus, a novel candidate endophenotype of psychiatric disorders. *Mol Brain* **1**, 6.

Zamanillo, D., Sprengel, R., Hvalby, O., Jensen, V., Burnashev, N., Rozov, A., Kaiser, K.M., Köster, H.J., Borchardt, T., Worley, P., L"A bke, J., Frotscher, M., Kelly, P.H., Sommer, B., Andersen, P., Seeburg, P.H. & Sakmann, B. (1999) Importance of AMPA receptors for hippocampal synaptic plasticity but not for spatial learning. *Science* **284**, 1805–1811.

Zhu, J.J., Esteban, J.A., Hayashi, Y. & Malinow, R. (2000) Synaptic potentiation during early development: delivery of GluR4-containing AMPA receptors by spontaneous activity. *Nat Neurosci* **3**, 1098–1106.

Acknowledgments

We thank Yukari Yamada of the Laboratory for Technical Support, Medical Institute of Bioregulation, Kyushu University for performing the ES cell injection, Rie Funatsu for maintaining the mouse colonies and Naoko Tsunekawa of the Laboratory for Genetic Engineering and Functional Genomics, Frontier Technology Center, Kyoto University Faculty of Medicine for technical assistance of the behavioural analyses. This work was supported by grants-in-aid for Scientific Research on Priority Areas 'Applied Genomics', Scientific Research (A) and IBR-shien from the Ministry of Education, Culture, Sports, Science and Technology of Japan and a grant-in-aid for Scientific Research (A) from the Japan Society for the Promotion of Science.

Supporting Information

Additional Supporting Information may be found in the online version of this article:

Figure S1: Emotional behaviour in the elevated plus maze test. The total number of arm entries (a), the percentage of open arm entries (b), the distance travelled (c) and the percentage of time spent in the open arms (d) in the elevated plus maze test are shown ($n = 15$ each). No significant differences between GluR4$^{-/-}$ and GluR4$^{+/+}$ mice were found in the four parameters examined.

Figure S2: Anxiety-related behaviour in the light–dark transition. GluR4$^{-/-}$ and GluR4$^{+/+}$ mice ($n = 16$ each) were examined for four parameters: total distance travelled (a), total time spent in the lit compartment (b), the numbers of transitions (c) and latency to the first transition (d). Only the number of transitions was lower in GluR4$^{-/-}$ mice than controls (c, $P = 0.0004$).

Figure S3: Home-cage activity in GluR4$^{-/-}$ mice. Two animals of the same genotype were put in a cage and their activity was monitored over approximately 7.5-day period. (a) The home-cage activity of the GluR4$^{-/-}$ mice was similar to that of the GluR4$^{+/+}$ mice ($n = 8$ each). Activity levels are expressed in arbitrary units integrated for each hour. (b) The social interaction was expressed as the number of particles in the image of the cage as viewed by automatic detection. When the animals were separated, two particles were seen, and when they were together, only one was observed. Each dot indicates mean per hour. There was no difference in the social interaction with their cagemate between the GluR4$^{-/-}$ and GluR4$^{+/+}$ mice.

Figure S4: Social interaction test in GluR4$^{-/-}$ mice. The total duration of contact (a), number of contacts (b), total duration of active contacts (c), mean duration per contact (d) and distance travelled (e) are shown (pairs of GluR4$^{-/-}$ mice: $n = 7$; pairs of GluR4$^{+/+}$ mice: $n = 8$). Only the mean duration per contact increased in the GluR4$^{-/-}$ mice (d, $P = 0.0283$).

Figure S5: Intact learning and memory in GluR4$^{-/-}$ mice in the eight-arm radial maze. The learning ability of GluR4$^{-/-}$ mice was tested using an eight-arm radial maze. The number of different arms chosen within the first eight choices (a), number of revisiting errors (b) and latency to obtain all pellets (c) are shown. No significant differences between the GluR4$^{-/-}$ and GluR4$^{+/+}$ mice were found in any of the parameters examined.

As a service to our authors and readers, this journal provides supporting information supplied by the authors. Such materials are peer-reviewed and may be re-organized for online delivery, but are not copy-edited or typeset. Technical support issues arising from supporting information (other than missing files) should be addressed to the authors.

JBC Papers in Press. Published on October 28, 2009 as Manuscript M109.066373
The latest version is at http://www.jbc.org/cgi/doi/10.1074/jbc.M109.066373

STRUCTURAL AND DYNAMIC FEATURES OF THE MUTT PROTEIN IN THE RECOGNITION OF NUCLEOTIDES WITH THE MUTAGENIC 8-OXOGUANINE BASE*

Teruya Nakamura, [1] Sachiko Meshitsuka, [2] Seiju Kitagawa, [2] Nanase Abe, [2] Junichi Yamada, [2] Tetsuya Ishino, [2] Hiroaki Nakano, [2] Teruhisa Tsuzuki, [3] Takefumi Doi, [2] Yuji Kobayashi, [2] Satoshi Fujii, [4] Mutsuo Sekiguchi [5] and Yuriko Yamagata [1]

From [1]Graduate School of Pharmaceutical Sciences, Kumamoto University, Kumamoto 862-0973, Japan, [2]Graduate School of Pharmaceutical Sciences, Osaka University, Suita 565-0879, Japan, [3]Graduate School of Medical Sciences, Kyushu University, Fukuoka 812-8582, Japan, [4]School of Pharmaceutical Sciences, University of Shizuoka, Shizuoka 422-8526, Japan, [5]Fukuoka Dental College, Fukuoka 814-0193, Japan

Running head: Crystal structures of MutT in the apo and 8-oxo-dGMP complex forms

Address correspondence to: Yuriko Yamagata, Graduate School of Pharmaceutical Sciences, Kumamoto University, 5-1 Oe-honmachi, Kumamoto 862-0973, Japan, Tel/Fax: +81-96-371-4638; E-mail: yamagata@gpo.kumamoto-u.ac.jp

Escherichia coli **MutT hydrolyzes 8-oxo-dGTP to 8-oxo-dGMP—an event that can prevent the misincorporation of 8-oxoguanine opposite adenine in DNA. Of the several enzymes that recognize 8-oxoguanine, MutT exhibits high substrate specificity for 8-oxoguanine nucleotides; however, the structural basis for this specificity is unknown. The crystal structures of MutT in the apo and holo forms and in the binary and ternary forms complexed with the product 8-oxo-dGMP and 8-oxo-dGMP plus Mn^{2+}, respectively, were determined. MutT strictly recognizes the overall conformation of 8-oxo-dGMP through a number of hydrogen bonds. This recognition mode revealed that 8-oxoguanine nucleotides are discriminated from guanine nucleotides by not only the hydrogen bond between the N7-H and Oδ (N119) atoms but also by the *syn* glycosidic conformation that 8-oxoguanine nucleotides prefer. Nevertheless, these discrimination factors cannot by themselves explain the roughly 34,000-fold difference between the affinity of MutT for 8-oxo-dGMP and dGMP. When the binary complex of MutT with 8-oxo-dGMP is compared to the ligand-free form, ordering and considerable movement of the flexible loops surrounding 8-oxo-dGMP in the binary complex are observed. These results indicate that MutT specifically recognizes 8-oxoguanine nucleotides by the ligand-induced conformational change.**

Although spontaneous mutations are indispensable to the evolutionary process of living organisms, they can also be lethal to the organism. Among the various modified bases in DNA, RNA, and nucleotides, 8-oxoguanine (8-oxoG)—a damaged form of guanine (G) generated by reactive oxygen species—is known to have highly mutagenic potency because of its mispairing with adenine. Therefore, organisms have an error avoidance pathway for preventing mutations caused by 8-oxoG. The *Escherichia coli* MutT protein (129 amino acids, M_r = 14,900) hydrolyzes 8-oxo-dGTP and 8-oxo-GTP to their corresponding nucleoside monophosphates and inorganic pyrophosphate in the presence of Mg^{2+} (1,2). Because 8-oxo-dGTP and 8-oxo-GTP can be misincorporated opposite adenine by DNA and RNA polymerases, the hydrolysis of the damaged nucleotides by MutT can avoid replicational and transcriptional errors. In DNA, 8-oxoG paired with cytosine is excised by MutM, an 8-oxoG DNA glycosylase, while MutY, an adenine DNA glycosylase, removes adenine paired with 8-oxoG (3-6).

The substrate specificities of enzymes that recognize 8-oxoG are quite varied. MutT exhibits high substrate specificity for 8-oxoG nucleotides; that is, the K_m for 8-oxo-dGTP is 14,000-fold lower than that for dGTP (7). In contrast, human MutT homologue 1 (hMTH1) hydrolyzes not only 8-oxo-dGTP but also several oxidized purine nucleotides such as 2-oxo-dATP, 2-oxo-ATP, 8-oxo-dATP, and 8-oxo-ATP. In terms of the hydrolysis of 8-oxo-dGTP, the K_m of hMTH1 for 8-oxo-dGTP is only 17-fold lower than that for dGTP (8,9). The solution structure

of hMTH1 as determined by nuclear magnetic resonance (NMR) has revealed its overall architecture and possible substrate-binding region (10); however, the broad substrate recognition mechanism of hMTH1 remains to be elucidated. MutM and MutY also have low specificity for 8-oxoG. For example, MutM can recognize a variety of damaged bases such as formamidopyrimidine, 5-hydroxycytosine, and dihydrouracil in addition to 8-oxoG (11-13), and MutY shows a kinetic preference for A:8-oxoG that is only 6-fold greater than that for A:G (14).

The crystal structures of OGG1, MutM, and MutY complexed with 8-oxoG-containing DNA (13,15,16) have revealed that, interestingly, OGG1 and MutM do not recognize the O8 atom, which is the most characteristic feature of the 8-oxoG moiety, and the interaction observed between the O8 atom and the main chain atom of MutY is relatively weak. Alternatively, OGG1, MutM, and MutY commonly discriminate 8-oxoG from G by the protonation at N7 accompanied by the oxidation of C8. Structural studies on various enzymes that recognize 8-oxoG have succeeded in explaining the mechanism by which 8-oxoG is discriminated from normal G in DNA, but one of the most interesting questions to be elucidated is the mechanism by which MutT acquires extremely high substrate specificity for 8-oxoG compared to the other enzymes.

MutT belongs to the Nudix (nucleoside diphosphate linked to some other moiety, X) hydrolase family (17). Nudix family members have a highly conserved MutT signature (Nudix motif); i.e., $GX_5EX_7REUXEEXGU$, where U is a hydrophobic residue and X is any amino acid. Current genome analyses have found a large number of open reading frames containing the MutT signature, but their functions, i.e., their substrates, are not identified in the case of almost all these proteins because of a lack of homology outside the MutT signature. MutT is the most examined protein in this family. Its structure was first determined by NMR (18) and has greatly contributed to the study of the Nudix hydrolase family. NMR studies of MutT with its product, 8-oxo-dGMP, have predicted several recognition models of 8-oxo-dGMP (19). However, the precise recognition mechanism of 8-oxoG nucleotides remains unclear. Therefore, it is necessary to determine the crystal structures of MutT in order to explain the extremely high substrate specificity of MutT for 8-oxoG nucleotides.

Here, we present X-ray crystallographic analyses of the apo enzyme; the Mn^{2+}-bound holo enzyme (MutT-Mn^{2+}); the binary complex with 8-oxo-dGMP, a reaction product (MutT-8-oxo-dGMP); and the tertiary complex with 8-oxo-dGMP and Mn^{2+} (MutT-8-oxo-dGMP-Mn^{2+}). These structures have revealed the mechanism of the extremely high substrate specificity of MutT for 8-oxoG nucleotides and have allowed us to propose the exact roles of some conserved residues in the MutT signature.

EXPERIMENTAL PROCEDURES

Protein expression and purification— The *E. coli* strain BL21 (DE3) harboring a newly constructed pET8c/MutT plasmid was used for the expression of native and selenomethionine (SeMet)-substituted MutTs. Native MutT was overexpressed in Luria-Bertani (LB) broth, and SeMet MutT was overexpressed in LeMaster broth containing seleno-DL-methionine instead of methionine with sufficient amounts of isoleucine, lysine, and threonine to inhibit the methionine pathway (20,21). This condition was also present in the overexpression of SeMet hMTH1 (22). Purification of MutT was carried out by almost the same procedure (except that the hydroxylapatite column chromatography step was skipped), as described previously (23). Diethylaminoethyl (DEAE) Sepharose and the HiPrep 16/60 Sephacryl S-200 HR column were substituted for DEAE Sephacel and the Sephadex G75 column, respectively. The purified protein solution was concentrated to approximately 6 mg/mL.

Crystallization— The native and SeMet-substituted apo forms and all complexes were crystallized by hanging-drop vapor diffusion at 288 K. Crystals of native and SeMet-substituted forms were obtained from a droplet containing 3 mg/mL protein, 10 mM Tris-HCl (pH 7.5), 0.5 mM ethylenediaminetetraacetic acid (EDTA), 2.5%

glycerol, 0.5 mM 2-mercaptoethanol, 0.7 M potassium sodium tartrate, and 44 mM 4-(2-hydroxyethyl)-1-piperazineethanesulfonic acid (HEPES)-NaOH (pH 7.5) equilibrated against a reservoir containing 1.4 M potassium sodium tartrate and 87 mM HEPES-NaOH (pH 7.5). Crystals of MutT-Mn^{2+} were obtained in the same manner, as described above, except that 10 mM $MnCl_2$ was added to the droplet. The crystallizations of MutT-8-oxo-dGMP and MutT-8-oxo-dGMP-Mn^{2+} were described previously (24). The crystals were transferred to a cryosolution of each reservoir containing 30% sucrose and were then flash-frozen.

Data collection, processing, phasing, and structure refinement— Diffraction data were collected at 100 K on beamlines 18B of Photon Factory (Tsukuba, Japan) and on beamlines 41XU, 44XU, 38B1, and 40B2 of SPring-8 (Harima, Japan). The data of native and SeMet-derivative forms were processed and scaled by DSP/MOSFLM and SCALA (25). The data of MutT-Mn^{2+} was processed and scaled by DENZO and SCALEPACK (26). There are two molecules in the asymmetric unit with V_M of 2.2 (native MutT) and 2.5 (MutT-Mn^{2+}) $Å^3 \cdot Da^{-1}$ (27). Data collection statistics of the best data used for structure determination and refinements are listed in Table 1. Data collection statistics of MutT-8-oxo-dGMP and MutT-8-oxo-dGMP-Mn^{2+} are quoted from the reference by Nakamura et al., 2004 (24).

The positions of eight selenium atoms were determined using SOLVE (28). The initial phases were calculated using MLPHARE (29) and improved using DM (30). The initial model was built using TOM (31) and O (32). The model was refined using X-PLOR (33) and CNS (34). Using the model of SeMet derivative, the successive refinement of native MutT converged at an R value of 20.4% and an R_{free} of 23.1% for reflections in the resolution range 20–1.8 Å. The structure of MutT-8-oxo-dGMP was solved by molecular replacement with AMoRe (35) using the structure of the native apo form as a search model. The $2F_o - F_c$ maps after CNS refinements clearly showed the density for 8-oxo-dGMP and the conformationally changed loop regions (L-A and L-D). These regions were manually built and fitted into the density with O.

The structure of MutT-8-oxo-dGMP-Mn^{2+} was refined starting with the coordinates of the MutT-8-oxo-dGMP. The structure of MutT-Mn^{2+} was solved by molecular replacement with AMoRe by using the structure of the apo form as a search model. The stereochemical qualities of the structures were checked by PROCHECK (36); the refinement statistics are listed in Table 2. Superposition of MutT structures were carried out using Lsqkab (37). All molecular graphics were prepared using PyMOL (38).

RESULTS AND DISCUSSION

Overall structures of MutT and MutT-8-oxo-dGMP— The crystal structures of the MutT apo and MutT-8-oxo-dGMP complex forms were determined at a resolution of 1.8 and 1.96 Å, respectively. MutT is composed of two α-helices (α-1 and α-2) and six β-strands (β-1 to β-6) (Fig. 1 and 2A); it adopts an α-β-α sandwich structure that is conserved among members of the Nudix family. The Nudix motif (23 residues from Gly38 to Leu60), i.e., the MutT signature ($GX_5EX_7REUXEEXGU$), adopts the characteristic strand-loop-helix-loop (SLHL) structure formed by β-3′, L-B, α-1, and L-C (39,40). The crystal of the apo form contains two protein molecules per asymmetric unit, and they are very similar to each other with root-mean-square deviation (rmsd) of 0.5 Å for the corresponding 121 Cα atoms. For simplicity, only one molecule will be referred to in all further discussions. MutT exists as a monomer, which is found in the MutT-8-oxo-dGMP crystal.

In the apo form, the electron densities of L-A connecting β-2 and β-3 are not available, indicating that the L-A loop region has a highly flexible conformation (Fig. 2A). On the other hand, in the MutT-8-oxo-dGMP complex, the ordering of the flexible L-A loop by interactions with 8-oxo-dGMP is observed (Fig. 2B, C). The plot of the displacement between the Cα atoms of the apo and complex forms is shown in supplemental Fig. S1A. The movements of the L-A and L-D regions are large (ca. 8~10 Å) (Fig. 2C, S1A). Except for these loop regions, the two forms have a similar structure with rmsd of 0.9 Å for the corresponding 101 Cα atoms.

A structural similarity search performed by

the DALI server (41) using the coordinates of MutT-8-oxo-dGMP indicated that 62 proteins (154 protein data bank [PDB] IDs, 278 protein chains) are structural homologs of MutT with Z-scores of >6.0 and belong to the Nudix superfamily with the Nudix fold. The MutT structure, with two α-helices and six β-strands, comprises the smallest structural unit among members of the Nudix superfamily. Of 62 proteins, half have unknown functions. Structures that are highly similar to the MutT complex form are the monomer structures of *Bdellovibrio bacteriovorus* RNA pyrophosphohydrolase; i.e., BdRppH in the ternary and binary forms complexed with GTP and Mg^{2+} (BdRppH-GTP-Mg^{2+}, 3FFU, rmsd = 1.8 Å, Z = 19.0) and with dGTP (BdRppH-dGTP, 3EF5, rmsd = 1.9 Å, Z = 18.3) (40) and unknown proteins from *Bartonella henselae* (3HHJ, rmsd = 1.8 Å, Z = 19.8) and *Methanosarcina mazei* (3GRN, rmsd = 2.1 Å, Z = 17.5), respectively. In MutT, the rmsd is rather large: 3.3Å for 120 Cα atoms between the X-ray and NMR structures in the ligand-free form and 3.5Å for 127 Cα atoms between structures in the complex form (PDB ID: 1MUT and 1PUS) (18,19).

Recognition scheme of 8-oxo-dGMP by MutT— When 8-oxo-dGMP binds to MutT, large ligand-induced conformational changes occur in the L-A and L-D regions, namely, the ordering of the flexible L-A loop and considerable movement of L-A and L-D to the surrounding 8-oxo-dGMP (Fig. 2C, 3A). The side chains of Arg23 and His28 on L-A form hydrogen-bonding interactions with phosphate and sugar moieties of 8-oxo-dGMP, respectively, whereas Arg78 interacts with the sugar moiety through a water-mediated hydrogen bond. Asp77 and Arg78 make two hydrogen bonds between their side chains. The conformational change of the L-A and L-D regions also produces the water molecule-mediated interaction between His28 and Asp77 and the CH-π interaction between His28 and Phe75 (Fig. 3A, S2). Thus, the loops L-A and L-D connect to each other, resulting in the formation of a cave composed of β-1, β-3, β-3′, β-5, and α-2 for substrate binding (Fig. 3B). 8-Oxo-dGMP is inserted deeply into the cave in which the wall on one side is filled with hydrophobic residues (Leu4, Ile6, Val8, Ile80, and Leu82), and the other side and bottom include some polar residues (Arg23 and Asn119). The 8-oxoG base and the deoxyribose are perfectly buried, and the phosphate group faces the solvents (Fig. 3B). The glycosidic conformation of 8-oxo-dGMP bound to MutT is *syn*. This fact is consistent with the first suggestion by Bessman et al. that MutT may recognize the syn conformation because the 8-substituted purine nucleotides were better substrates compared with the normal purine nucleotides (42). The sugar ring puckering and the sugar-phosphate backbone conformation of 8-oxo-dGMP are *C2′-end* and *gauche⁻-trans*, respectively. These conformations are generally observed in 8-substituted purine nucleosides and 5′-nucleotides (43).

These ligand-induced conformational changes result in the strict recognition of the overall structure of 8-oxo-dGMP by MutT through a number of hydrogen bonds (Fig. 3C). The characteristic features of the 8-oxoG base are the oxygen atom (O8) at C8 and the hydrogen atom (N7-H) at N7 accompanied by oxidation. MutT recognizes N7-H of 8-oxoG by a hydrogen bond with Oδ of Asn119 (Fig. 3C, a red dashed line). The 8-oxoG base is also recognized by hydrogen bonds with Asn119 and Phe35; i.e., the Nδ of Asn119 forms a hydrogen bond with O6 of 8-oxoG, and the main chain atoms of Phe35 participate in three types of hydrogen bonds with N2-H, N1-H, and O6. On the other hand, the O8 atom does not form hydrogen bonds with any amino acid residues although it does participate in the weak C-H---O interaction with the phenyl ring C-H of Phe75 (C---O distance, 3.4 Å) and the van der Waals interactions with the side chain C-H moieties of Phe75, Pro116, Leu82, Ile80, and Ala118 (Fig. 3D). In addition, the carbonyl oxygen of Gly37 forms water molecule-mediated hydrogen bonds with N2-H of 8-oxoG and the phosphate oxygen. The side chain of His28 is directly hydrogen-bonded to the O3′ atom of the deoxyribose. The O3′ atom also forms a hydrogen bond with a water molecule, binding to the side chain of Arg78. The phosphate group forms a hydrogen bond with the side chain of Arg23 and a water molecule-mediated hydrogen